Scientific Research

Contribution to the Petrography, Geochemistry, and Petrogenesis of Zarqa-Ma'in Pleistocene Alkali Olivine Basalt Flow of Central Jordan

Ibrahim Ahmad Ali Bany Yaseen

Institute of Earth and Environmental Sciences, Al-al-Bayt University, Al-Mafraq, Jordan
Email: ibanyyaseen@yahoo.com

Abstract

The Zarqa-Ma'in basalt (MB) occurs near a plateau basalt (wadi fills) covering about 15 km² of Makawir, Ataruz, and Hammat um Hasana cone areas in central Jordan. The tectonic evolution occurred through intraplate volcanism and erupted through fissure systems along the Dead Sea, transforming the fault during Miocene to Pleistocene period. Three stages of eruption of MB have been recorded during Pleistocene from 6 to 0.6 Ma. The petrographic analyses data show that the MB rocks are composed of plagioclase, olivine, pyroxene, and magnetite, including secondary minerals calcite, iddingsite, serpentine, and zeolite. Furthermore, the MB rocks have narrow ranges of major and trace element concentrations, and are of under saturated silica type and belong to sodic alkaline magma series. The geochemical characteristics of MB indicate that MB was derived from a slightly fractionated magma as reflected by its high MgO (6.3 - 11.7 ppm) concentration with Mg number from 0.41 to 0.61, low silica content (40.83 - 47.55 wt%), and high Cr and Ni concentrations (115 - 475 and 105 - 553 ppm, respectively). This basalt exhibited low degree of partial melting (10%) for garnet peridotite mantle source. The model mineral fractionation showed that the MB could be fractionated to clinopyroxene, orthopyroxene, olivine, and plagioclase.

Keywords

1. Introduction

The intraplate volcanic fields are generated and spread along the western margin of the Arabian Peninsula from Jordan, Syria, and Saudi Arabia. This intraplate volcanism occurred after the break of Africa and Arabia, opening the Red Sea and resulting in Oligocene flood volcanism in Yemen and Ethiopia [1] [2]. Furthermore, an extensive late Cenozoic intraplate volcanism covers the central Jordan, which may reflect the lithosphere extension [3].

The present study was focused on the intraplate volcanic field in central Jordan (Zarqa-Ma'in area). Volcanism in Jordan occurs as sporadic small volcanic centers along the eastern side of the Dead Sea plate boundary (**Figure 1**). These volcanoes are clearly associated with continental rifting and inception of the Dead Sea plate boundary. The relationship between magmatism and tectonic of the intraplate volcanism has been reported earlier [4], indicating that alkaline volcanism in Jordan is similar to the Arabian intraplate volcanic fields, which erupted through two main fissure systems along the eastern margin of the Dead Sea rift in the east-west direction [5] [6]. Furthermore, it has been reported that this volcanism might have probably commenced during the Miocene period and continued to Pleistocene [7]. Based on the K-Ar age, many researchers [4] [8]-[10] have divided the volcanic activity of Jordan into three episodes: Oligocene to early Miocene (26.23 - 22.17 Ma), Middle to late Miocene (13.97 - 8.94 Ma), and late Miocene to Pleistocene (6.95 - 0.15 Ma).

Previous petrochemical studies on the intraplate basaltic rocks in Jordan have indicated that the basaltic rocks are composed of alkali basalts and basanites [4]-[6] [11]-[14]. Furthermore, Regional Geochemical Prospecting Project reported five geochemical anomalous areas reflecting the highest concentration of elements in the Zarqa-Ma'in basalt (MB) [15].

The basalts in central Jordan have been found to occur in seven places, namely, Tafila, Wadi Dana, Jabel Shiihan, El-Lajjoun, Jurf Al-Darawish, Ghor Al-Katar, and Wadi Zarqa-Ma'in, in the form of plateau basalts, local flows (wadi fills), or individual volcanic bodies (cones, plugs, and dikes). Some doloritic dykes have also been observed to occur along the major faults, such as Wadi Al-Fayha fault zone, Wadi Dana, Tafila [16], and Shihan plateau [4]. The purposes of the current study were to investigate the petrography, geochemistry, and petrogenesis evolution of the intercontinental basaltic flow at Zarqa-Ma'in area, which is in the east of Dead Sea in central Jordan; to determine the origin and type of the parental magma; and to investigate the tectonic setting evolution of the MB region.

2. Geological Setting

The MB covers an area of about 16 km^2 along the boundary of Wadi Zarqa Ma'in, and is located at 31°30'496"N -

Figure 1. Location, geological and structural map (After Natural Resources Authority, 1997) of the study area.

31˚30'500"N and 35˚30'346"E - 35˚30'375"E. The areas of Makawir, Ataruz, and Hummat Um Hasana cones cover the sides of the Wadi Zarqa Ma'in faults along 9.5 km (**Figure 1**). Based on the K-Ar age dating, Pleistocene basalts are divided into three stages of eruption [9] [10] [16]-[18]. In the present study, the geomorphology of the study area provided evidences of three stages of eruption flows: The first stage (6 Ma) consisted of angular fragments of altered basalt mixed with older sediments at the bottom of the Wadi Zarqa-Ma'in; the second stage (3.4 Ma) was induced by basaltic dykes cutting the basal breccia cones overlying this breccia; and the last stage (0.6 Ma) of eruption lava flows covered the recent alluvium in the wadi [19] [20].

The MB has been considered to have many different structures, depending on lava consolidation. The dominant MB structure, such as blocky basalt, has low viscosity and crystallizes rapidly. In Jabel Mukawir, scoria bombs within the scoria ash and pyroclastic have been noted to be smaller in size [19]. The cellular basalt structure develops into the shape of gas cavities in the direction of the lava flow. Vesicular basalts are elongated, rounded or semi rounded with a vesicular texture, and secondary minerals such as calcite and zeolite partially fill these vesicles giving an amygdaloidal texture. The Zarqa-Ma'in fault is the main fault in the study area along the east-west direction, and extends from the Dead Sea to Wadi Sirhan. The basalt intrudes along the fault and forms a volcanic neck. The MB occurs in the direction of N-S, E-W, NW-SE, and NE-SW, which coincide within the main regional and local structural fault directions (**Figure 1**). The N-S trending fractures are parallel to the Dead Sea transform fault, whereas the E-W fractures lie parallel to Zarqa-Ma'in fault, Suwaqa fault, Hasa fault, and Salwan fault perpendicular to the Dead Sea Transform Fault and Suwaqa normal fault [21]. The NE-SW trending joints are consistent with the late Pan-African stress pattern and are parallel to Amman Hallabat fault [22] [23]. The NW-SE trending direction is related to the regional faults, such as Karak Fayha fault zone and Wadi Sirhan fault system, which extends from Saudi Arabia in the south continuing to north Jordan (**Figure 1**) [24].

3. Sampling and Analytical Techniques

A total of 26 representative rock samples from the MB were crushed and powdered using geochemical techniques. The major elements were analyzed on fused glass discs-like pellet (bead) by using a Phillips X-Ray Florescence Spectrometry (XRF) Majex PW-2424 Model at the Al al-Bayt University. A total of 2 g of the powder samples were mixed with 8 g of lithium tetra borate and fused in platinum crucibles over gas burners (1000˚C) for 1 h. The melts were poured into a mold to create glass disks. The Loss on Ignition (LOI) was determined by the weight lost after melting at 1000˚C. The trace elements were analyzed by decomposition using Ione Conductive Coupled Plasma Emission Spectroscopy (ICP-AES) at Natural Resources Authority Labs. Thin section prepared at the University of Jordan and examined under polarizer microscope. Photomicrographs of the samples were obtained by using LEICA-DMEP Canon camera in the petrography unit at Natural Resources Authority. The geochemical data were processed and pictorially represented by using the computer program Igpet 32. CIPW-Norm calculations were carried out by using the Excel sheet [25].

4. Results

4.1. Petrography and Mineralogy

The MB samples were melanocritic, holocrystalline, hypidiomorphic fine to medium grained and exhibited aphentic to porphyritic texture, with elongated and oval-shaped vesicles. The main mineral constituents were plagioclase, olivine, pyroxene, and opaque minerals (mainly magnetite). The secondary minerals included calcite, iddingsite, serpentine, and zeolite. The common textures of the MB were trachytic, glomeroporphyritic, vesicular, and amygdaloidal.

4.1.1. Plagioclase
Plagioclase occurred in two generations as larger phenocrysts and as small tablature to elongated microlites inthe ground mass. The phenocrysts were anhedral laths from 0.5 to 5 mm in length, forming about 32% - 47% vol% of the rock. The crystals showed simple twining. The extinction angles on plagioclase phenocrysts ranged from 26˚ to 31˚, indicating a labradorite composition (An50-An70), which was determined by using the method described by [26]. The plagioclase elongated crystals exhibited orientation similar to those of olivine and pyroxene crystals, presenting a trachytic texture (**Figure 2(a)**). The glomerophyritic texture (plagioclase, pyroxene, and olivine enclosed in fine-grained ground mass) was noted in clusters of four crystals (**Figure 2(b)**). Seritiza-

tion was observed along the boundary of the crystals as yellow to turbid rims. Albite plagioclase was also recorded, which was formed by conversion of Ca-plagioclase to Na-plagioclase as a result of instability of Ca-plagioclase during weathering.

4.1.2. Olivine

Olivine occurred as euhedral to subhedral and round-shaped phenocrysts, ranging between 2 and 6 mm in diameter, in the ground mass. The olivine crystals were colorless to pale gray color, displaying seriate texture, with high degree of alteration to iddingsite (**Figure 2(c)**). The aggregates exhibited glomeroporphyritic texture (**Figure 2(b)**). The larger crystals were slightly and moderately fractured. Iddingtization was common particularly along the edge and fractures of the crystals. Some crystals were partially to completely pseudomorphosed to brown iddingsite (**Figure 2(c)**). The altered products were considered to have resulted from the relatively low-temperature deuteric alteration process [14] and embayment of olivine crystals as a result of interaction between melt and olivine crystals during the crystallization process [27].

The normal olivine content in the MB ranged from 3.32 wt% to 14.85 wt%, with an average of 9.43 wt% (**Table 1**), which corresponded to the olivine modal value of 10 vol% - 20 vol%. The normative average diopside content was 20.38 wt% and the average nepheline content was 3.75 wt%, which allowed classifying the rocks as alkali olivine basalt and basanite (olivine > 10%) [28].

4.1.3. Pyroxene

Pyroxene occurred as colorless to gray pale brown color, anhedral to subhedral crystals, comprising about 12 vol% - 17 vol%. The crystals had a size between 0.3 and 5 mm, with perfect parallel cleavage (110), which intersected at 90° in the cross-section. The pyroxene crystals had an inclined extinction between 48° and 54°, indicating the presence of clinopyroxene of augite. The pyroxene intersected with plagioclase crystals to form ophitic to sub-ophitic texture (**Figure 2(b)**), and the crystal zoning was present in clinopyroxene (**Figure 2(d)**). The pyroxene crystals were affected by alteration (hydrothermal alteration), which resulted in serpentine fibrous crystals of chlorite green to pale green color.

4.1.4. Opaque Minerals

Opaque minerals were commonly found in MB, forming about 5 vol% - 8 vol% of the rocks and ranging from 0.2 to 3 mm in size. They mostly occurred as magnetite phenocrysts scattered throughout the rock and as inclusion within olivine and pyroxene crystals (**Figure 2(c)** and **Figure 2(d)**). The optical properties of magnetite were black color with PPL and XPL optics.

4.1.5. Vesicles

The MB showed ellipsoidal to void and elongated vesicles. The long axis was about 10 mm long and 5 mm width. The vesicles were filled with secondary minerals, calcite and zeolite (**Figure 2(e)**), and formed about 3 vol% - 7 vol% of the rock.

4.1.6. Groundmass

The groundmass of MB consisted of plagioclase (labrodorite), olivine, pyroxene (augite), and opaque minerals (mainly magnetite), with secondary minerals such as iddingsite, calcite, zeolite, and chlorite.

## 4.2. Rock Geochemistry

4.2.1. Major Oxides

The results of sample analyses (**Table 1**) were expressed in weight percent (wt%) for major element oxides and in part per million (ppm) for trace elements. The major elements ranged from 99.00% to 100.90%, which were within the limit of analytical methods. All the samples were relatively similar in composition, which was evident from the very narrow ranges of major and trace element concentrations. The range of the silica content was narrow between 40.83% and 47.55 wt% with an average of 44.96 wt%, which is within the average value reported for alkali basalt and basanite by many other authors [5] [13] [14] [29]-[32].
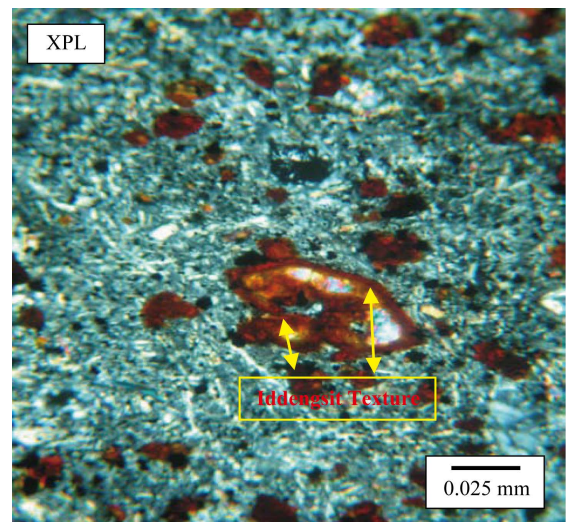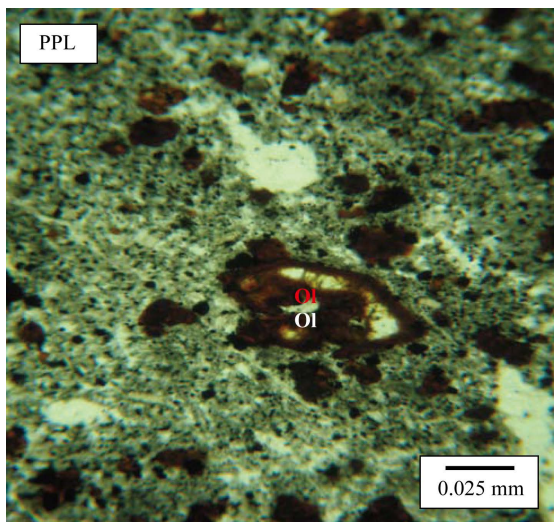
The MgO content of the MB ranged from 6.3 wt% to 11.7 wt% with an average of 9.04 wt%. The Mg number (Mg≠), defined as the molecular proportion of $Mg^{2+}/(Mg^{2+} + Fe^{2+})$ [33] [34], is usually used as a petrogenetic
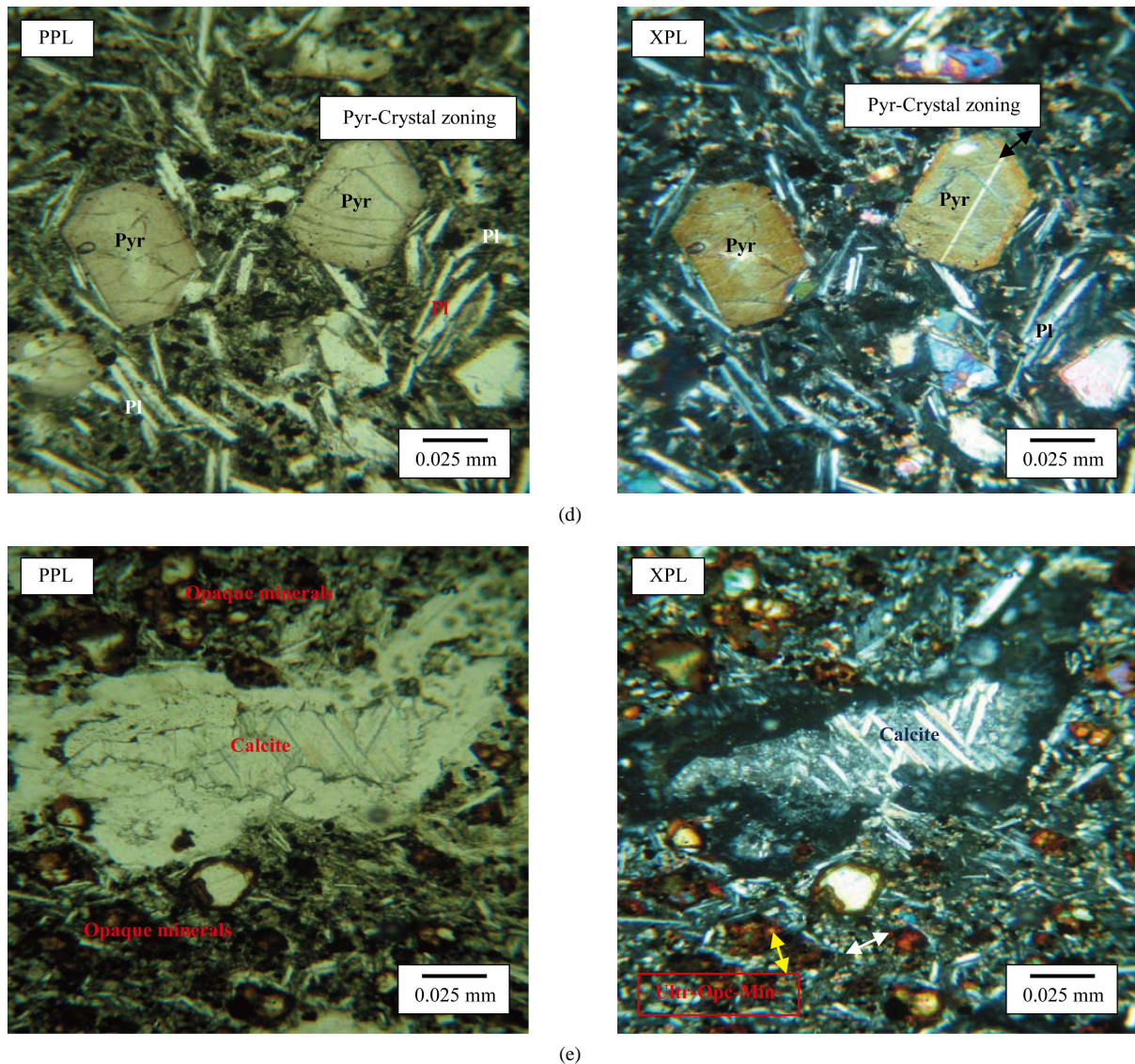
(a)

(b)

(c)

(d)

(e)
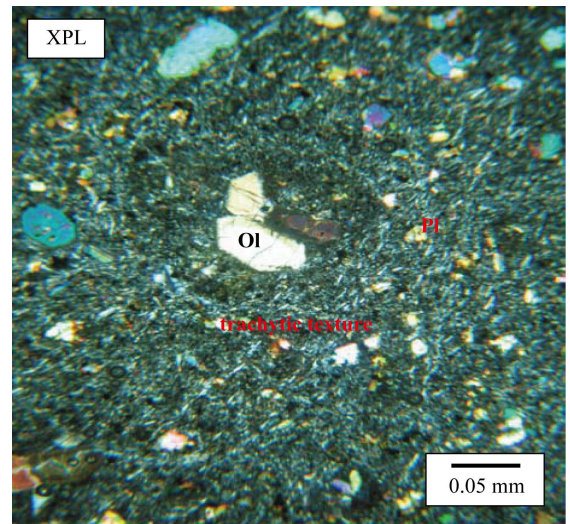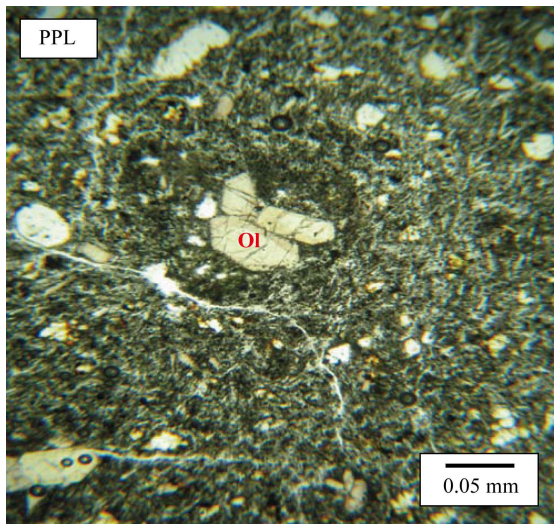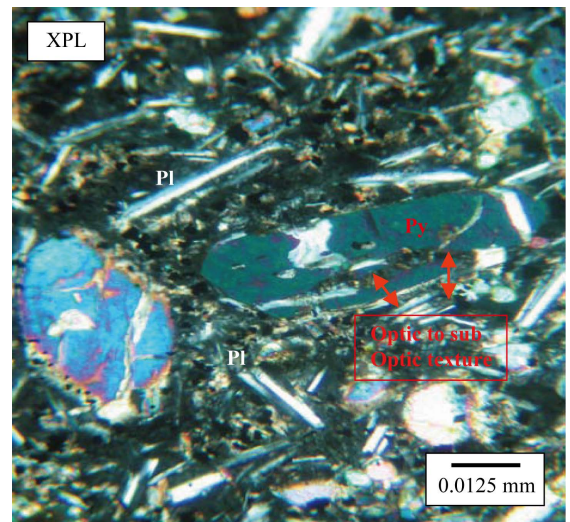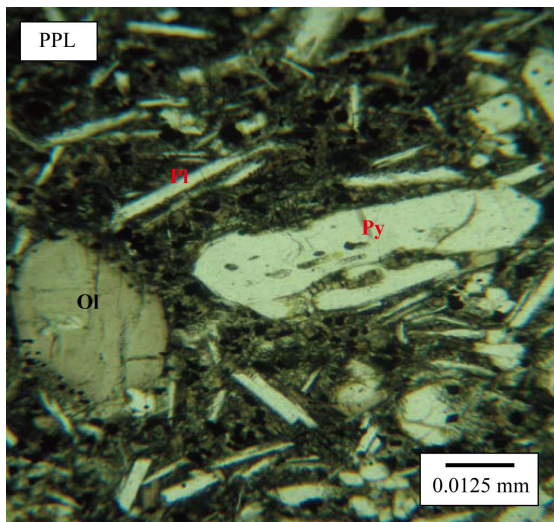
Figure 2. Photomicrographs of the MB studied. (a) Trachytic texture, with plagioclase fine crystal surrounding olivine crystals (magnification 4×, Sample No. MB9); (b) Glomeroporphyritic texture, exhibiting the porphyritic texture of phenocrysts in the aggregates called glomerocrysts or crystal clots. Glomeroporphyritic texture is common in plagioclase and pyroxene crystals (magnification 20×, Sample No. MB1); (c) Euhedral olivine crystal with high iddingsite alteration and showing opaque minerals (magnification 10×, Sample No. MB10); (d) Porphyritic texture, with subhedral to anhedral clinopyroxene crystals appearing in the crystal zoning and exhibiting opaque minerals (magnification 10×, Sample No. MB1); and (e) Vesicular basalt filling with calcite mineral to produce amygdaloidal texture and opaque mineral (magnetite) alteration to iron oxide (magnification 10×, Sample No. MB8). Ol: olivine; Pyr: pyroxene; Pl: plagioclase; Opc: opaque minerals; magnification 4×, 0.05 mm; magnification 10×, 0.025 mm; magnification 20×, 0.0125 mm.

indicator for magma fractionation and its primitive volcanic rocks [35]. The MB exhibited a high Mg≠, ranging between 0.41 and 0.61, with an average of 0.52. The Mg≠ calculation considers the Fe content in the rocks. It has been reported that values of Mg≠ > 0.7 can be considered as a threshold that characterizes primitive magmas [36]. In [37], it has been suggested that a Mg≠ of 0.65 is a distinct value. Moreover, the Fe content of the MB ranged between 7.36 wt% and 15.42 wt%, with an average of 12.93 wt%, indicating that the rocks were enriched in Fe. In a previous study [5], it was suggested that SiO_2 under saturated magma had a high FeO content of >11 wt% and high MgO content of >7. In [35] [38], it has been reported that rocks with high Mg# (>60) exhibit lowest contents of Nb and Zr and higher contents of Cr and Ni.

Table 1. Chemical composition of the samples from MB. The major oxides are given in wt%, trace elements in ppm and CIPW-wt% norm.

Sample No.	Mb1	Mb2	Mb3	Mb4	Mb5	Mb6	Mb7	Mb8	Mb9	Mb10	Mb11	Mb12	Mb13
SiO_2	45.90	45.04	44.70	46.22	40.83	46.50	45.50	45.95	43.94	45.84	43.12	44.92	44.81
TiO_2	2.30	2.74	2.77	2.83	1.54	2.70	2.87	2.72	2.58	2.69	2.72	2.41	2.79
Al_2O_3	10.40	12.05	13.21	12.93	10.12	13.48	13.3	12.39	11.42	11.65	11.81	11.75	12.77
Fe_2O_3	11.37	14.06	12.04	12.2	7.36	12.6	14.63	13.77	14.32	15.17	11.85	14.38	13.63
MnO	0.14	0.17	0.17	0.29	0.03	0.05	0.05	0.08	0.95	0.04	0.06	0.05	0.07
MgO	10.26	10.4	8.98	8.63	9.23	9.05	8.8	8.27	10.3	9.98	9.56	9.6	7.38
CaO	12.7	8.14	9.93	8.16	23.4	8.02	7.4	9.43	8.2	7.1	15.2	7.75	11.2
Na_2O	3.2	3.95	4.01	3.59	4.36	4.12	3.95	3.86	4.51	3.96	3.12	4.31	3.46
K_2O	1.47	1.46	1.51	1.53	0.84	0.9	1.18	1.39	0.95	0.87	0.95	1.08	0.71
P_2O_5	0.25	0.35	0.39	0.28	0.36	0.41	0.32	0.27	0.29	0.31	0.23	0.41	0.29
LOI	2.21	2.13	2.51	2.97	2.31	2.11	2.41	1.98	2.22	1.82	1.82	2.51	2.25
sum	100.2	100.5	100.2	99.63	100.4	99.9	100.4	100.1	99.7	100.4	100.4	99.2	99.4
Mg#	0.41	0.55	0.56	0.55	0.61	0.55	0.51	0.51	0.55	0.53	0.34	0.53	0.48
Na_2O/K_2O	2.17	2.70	2.65	2.34	5.19	4.57	3.34	2.77	4.74	4.55	3.28	3.99	4.87
Al_2O_3/TiO_2	4.52	4.39	4.76	4.56	6.57	4.99	4.63	4.55	4.42	4.33	4.34	4.87	4.57
Cr	163	224	216	250	115	280	244	235	237	282	259	324	243
Co	39	57	51	57	38	56	54	53	60	51	53	57	55
Ni	324	413	419	400	223	386	387	457	509	395	257	457	337
Cu	42	57	50	58	46	63	62	73	66	55	59	37	60
Zn	106	125	124	130	74	109	127	119	123	140	147	137	144
Sr	938	795	884	934	676	698	889	1276	805	857	859	647	881
Y	16	19	19	20	12	14	20	19	17	18	17	17	17
Nb	47	40	45	47	27	42	44	47	38	44	51	33	46
La	35	36	40	42	13	29	35	36	36	39	36	26	40
Ce	71	63	74	77	45	54	61	62	59	70	73	41	79
Pb	17	19	6	9	12	7	10	7	4	9	10	27	13
Ba	628	357	381	480	188	364	334	954	292	347	352	229	400
Zr	280	265	262	297	250	249	296	267	180	418	220	242	483
Cr/Ni	0.503	0.542	0.516	0.625	0.516	0.725	0.630	0.514	0.460	0.714	1.008	0.709	0.721
Zr/Nb	8.26	6.63	5.82	6.32	25.89	8.31	6.73	7.81	12.03	9.50	9.82	12.85	10.50
Zr/Y	24.25	13.95	13.79	14.85	58.25	24.93	14.80	19.32	26.88	23.22	29.47	24.94	28.41
Y/Nb	0.34	0.48	0.42	0.43	0.44	0.33	0.45	0.40	0.45	0.41	0.33	0.52	0.37

Continued

Sample No.	Mb14	Mb15	Mb16	Mb17	Mb18	Mb19	Mb20	Mb21	Mb22	Mb23	Mb24	Mb25	Mb26
SiO_2	44.95	44.94	43.8	43.68	45.85	45.65	44.55	45.76	43.36	44.89	47.55	44.89	43.97
TiO_2	2.86	3.00	3.07	3.30	2.80	2.55	2.60	2.40	2.30	1.50	1.50	2.56	1.93
Al_2O_3	12.45	13.8	11.36	12.36	12.14	12.47	12.86	13.87	10.9	12.50	13.61	11.45	9.98
Fe_2O_3	12.50	14.30	15.42	14.33	14.3	13.46	13.70	11.80	13.60	12.00	11.40	12.58	9.44
MnO	0.15	0.13	0.17	0.16	0.14	0.16	0.18	0.11	0.25	0.18	0.16	0.21	0.42
MgO	8.85	9.50	8.70	7.50	8.20	8.85	8.5	8.87	11.7	10.2	8.82	8.5	6.3
CaO	9.94	7.34	9.70	12.6	8.52	7.95	8.96	9.25	10.1	10.5	9.2	11.8	20.9
Na_2O	3.14	3.65	4.34	3.92	3.31	4.41	3.92	4.27	4.1	4.26	4.37	3.26	3.12
K_2O	1.30	1.40	1.50	1.54	1.30	1.20	1.61	0.55	0.84	0.63	0.66	1.87	0.79
P_2O_5	0.27	0.31	0.28	0.29	0.22	0.26	0.33	0.23	0.25	0.22	0.19	0.21	0.27
LOI	2.62	1.69	1.96	1.21	2.31	2.21	1.96	2.34	2.57	2.17	1.83	2.1	2.87
sum	99.0	100.1	100.3	100.9	99.19	99.2	99.2	99.5	99.8	99.1	99.3	99.4	99.9
Mg#	0.55	0.53	0.52	0.47	0.50	0.53	0.52	0.57	0.60	0.59	0.57	0.54	0.53
Na_2O/K_2O	2.41	2.60	2.89	2.54	2.54	3.67	2.43	7.76	4.88	6.76	6.62	1.74	3.94
Al_2O_3/TiO_2	4.35	4.60	3.70	3.74	4.33	4.89	4.94	5.77	4.73	8.33	9.07	4.47	5.17
Cr	138	162	187	126	134	267	256	144	475	289	269	276	225
Co	38	54	60	44	58	45	57	35	58	51	45	47	65
Ni	271	306	553	543	270	486	164	105	425	257	242	221	537
Cu	55	47	45	51	52	54	75	54	39	65	54	85	64
Zn	121	138	153	135	141	126	137	98	126	98	94	117	144
Sr	920	1062	1055	971	962	963	765	815	767	477	529	645	723
Y	19	18	18	20	18	17	19	17	16	15	17	17	14
Nb	50	50	56	61	48	41	46	44	24	22	24	56	46
La	58	53	44	43	60	54	67	72	32	19	23	31	19
Ce	75	84	88	93	90	69	82	62	53	24	27	46	47
Pb	3	5	8	6	7	11	5	9	7	10	6	4	11
Ba	581	492	361	342	315	336	427	260	462	416	336	453	267
Zr	190	300	152	210	342	240	350	195	242	137	152	251	140
Cr/Ni	0.509	0.529	0.338	0.232	0.867	0.549	1.561	1.371	1.118	1.125	1.112	1.245	0.949
Zr/Nb	10.80	6.00	6.29	8.07	7.13	5.85	7.61	10.93	4.48	6.23	6.33	4.48	8.09
Zr/Y	28.42	16.67	19.56	24.60	19.00	14.12	18.42	28.29	15.30	9.13	8.94	14.76	26.57
Y/Nb	0.38	0.36	0.32	0.33	0.38	0.41	0.41	0.39	0.30	0.68	0.71	0.30	0.30

Continued

Sample No.	Mb1	Mb2	Mb3	Mb4	Mb5	Mb6	Mb7	Mb8	Mb9	Mb10	Mb11	Mb12	Mb13
An	10	11	13.9	15.13	9.23	16	15.7	12.62	8.3	11.7	15.67	9.85	18
Al	21	28.2	23.6	31..39		35.6	34.9	30.55	26.5	34.4	24.8	34.2	30.4
Or	8.9	8.86	9.16	9.33		5.43	7.26	8.4	5.8	5.25	5.67	6.61	3.72
Ol	3.4	12.2	9.67	11.63	4.4	12.9	13.1	8.47	11..65	12.4		12.5	6.21
Di	36	16.3	19.6	12.13	37.3	10.1	8.3	19.2	20.1	10.3	24.82	14.9	21.8
Ne	4	3.22	6		16.87			1.46	6.87		1.1	1.93	
Pe	3.7	3.55	4.42	0.13	2.6	1.22	1.24	4.47	2.54		4.56	4.07	3.77
He	13	14.4	12.3	12.61	7.82	12.9	13.1	14.03	14.7	15.5	15.06	14.9	14.1
Il	0.4	0.43	0.43	0.7	0.1	0.42	0.16	0.26	2.19	0.15	0.15	0.17	0.2
Ap	0.6	0.83	0.92	0.93	0.86	0.95	0.76	0.64	0.6	0.74	0.53	0.97	0.69
Sample No.	Mb14	Mb15	Mb16	Mb17	Mb18	Mb19	Mb20	Mb21	Mb22	Mb23	Mb24	Mb25	Mb26
An	16.6	17.43	7.2	11.65	14.91	11	13.11	17.53	9.1	13.53	15.97	11.32	11.24
Al	27.6	31.4	23.1	15.31	28.94	33.75	26.73	33.57	20.1	22.84	34.23	17.62	4.71
Or	7.98	8.4	9.1	9.1	7.92	7.33	9.81	3.36	5.1	3.84	4	11.35	4.79
Ol	10.1	14.85	7.78	3.3	6.37	10.9	9.64	10.8	12.04	9.68	9.43	5.28	
Di	18.3	6.16	23.57	30.25	14.15	15.52	17.28	15.83	26.34	26.76	19.58	30.64	34.87
Ne			7.73	9.73		2.57	4	1.98	8.43	7.8	2	5.81	12.18
Pe	2.9	1.88	4.88	5.22		4.1	4.2	4	3.48	2.25	2.3	4.1	2.46
He	13	14.54	15.68	14.38	14.78	13.88	14.1	12.15	13.96	12.4	11.7	12.93	9.72
Il	0.38	0.34	0.47	0.47	0.34	0.45	0.41	0.24	0.58	0.43	0.36	0.5	1.03
Ap	0.64	0.74	0.69	0.67	0.54	0.63	0.79	0.55	0.6	0.54	0.44	0.51	0.65

In the present study, it is suggested that all the above-mentioned evidences indicate that the rocks undergo a smaller degree of partial melting at high pressures. The MB had an average Na_2O and K_2O content of 3.86 and 1.15 wt%, respectively. The total $Na_2O + K_2O$ values were similar in all the samples, exhibiting an average value of 5.02 wt%. The average ratio of Na_2O/K_2O was 5.00, indicating the sodic affinity of the rocks (**Figure 3**), and that of Al_2O_3/TiO_2 was 4.93, which suggested the basic affinity of the rock.

4.2.2. Trace Elements

The MB was found to have a high content of Ni and Cr. The content of Ni varied between 105 and 553 ppm, with an average value of 359 ppm, suggesting the presence of olivine and clinopyroxene fractions in the MB [40]. The Cr content ranged from 115 to 475 ppm with an average value of 230 ppm and a Cr/Ni ratio of 0.23 - 1.56. The high content of Ni and Cr indicated that the parental magma had been derived through partial melting of peridotite mantle source [5] [36].

The Sr and Zr contents in the MB were relatively high, with Sr ranging from 477 to 1276 ppm (average of 838 ppm) and Zr ranging from 137 to 699 ppm (average of 357 ppm). The Nb content ranged between 22 and 61 ppm, with the average Zr/Nb ratio of 8.34. The Y content was very low, showing a very limited variation that ranged from 12 to 20 ppm, with an average Y/Nb ratio of 0.41. This ratio has also been reported earlier [41] for the intercontinental alkali basalt. The La content ranged between 13 and 72 ppm, with an average of 39 ppm,

while the Ce content ranged between 24 and 93 ppm, with an average of 64 ppm.

5. Discussion

The data on the major and trace elements of the MB were used to construct discriminated plots, which were applied for the classification, nomenclature, and interpretation of the tectonic setting of the MB. Based on [42], the samples plotted in the alkaline rock field (**Figure 4(a)**). In the AFM diagram, the samples plotted in the calc-alkaline series (**Figure 4(b)**). Based on [29], the samples of MB plotted in the basalt, trachybasalt, and tepherite basanite field (**Figure 5**). In the ternary diagram based on [41], Ti-Zr-Y was distinguished among island-arc tholeiitas, MORB, calc-alkaline, and intraplate basalt, and all the MB samples were plotted within the plate basalt field (**Figure 6(a)**). On the other hand, Ti-Zr-Sr of all the MB samples plotted in the calc-alkaline basalt field [41] (**Figure 6(b)**).
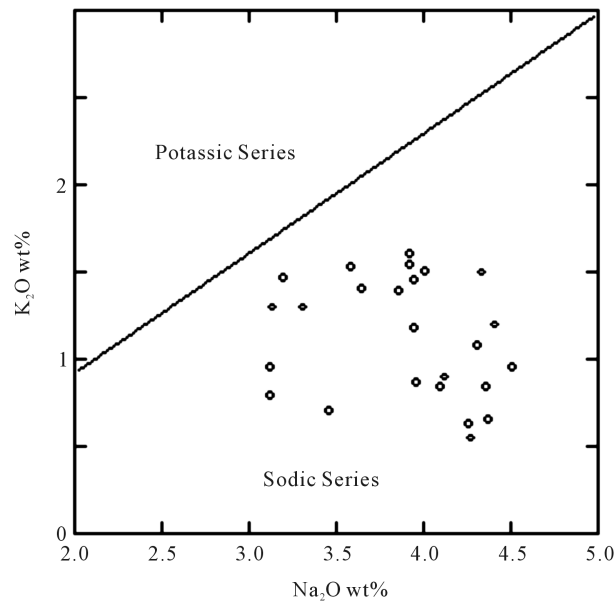
Figure 3. K_2O vs. Na_2O showing the sodic affinity of the MB samples [39].
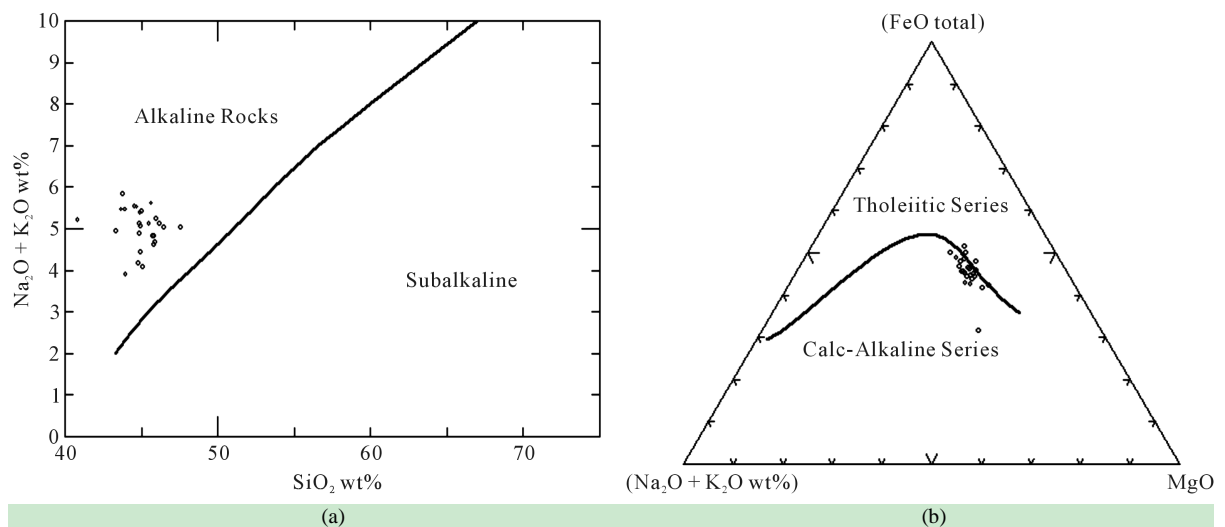
Figure 4. (a) Total alkali vs. SiO_2 in MB [42]; (b) AFM diagram showing the boundary between the calc-alkaline field and tholeiitic field for MB [42].
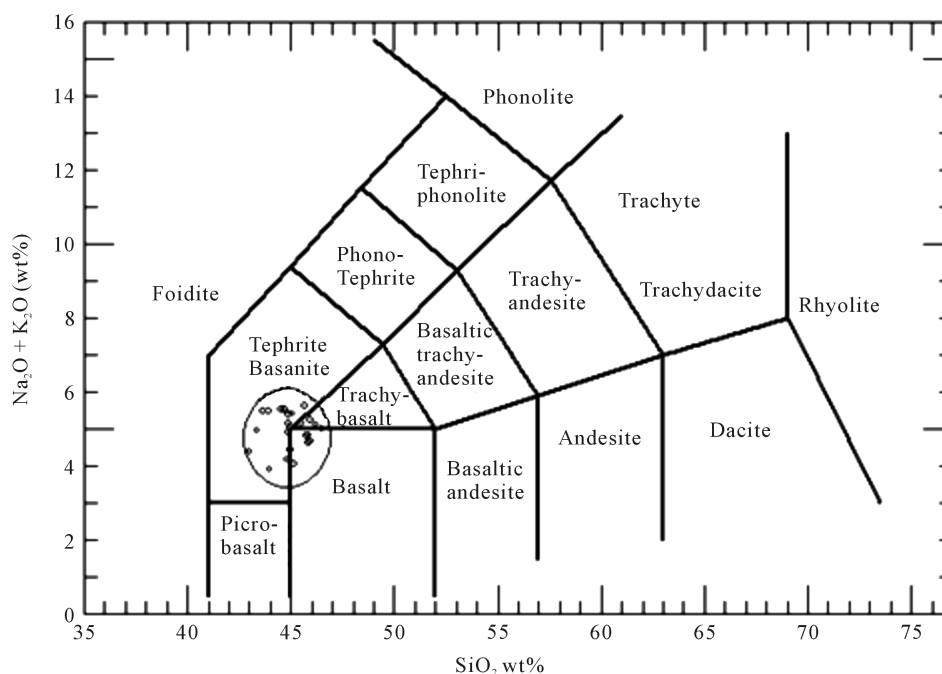
Figure 5. Chemical classification of MB alkali vs. silica [42].
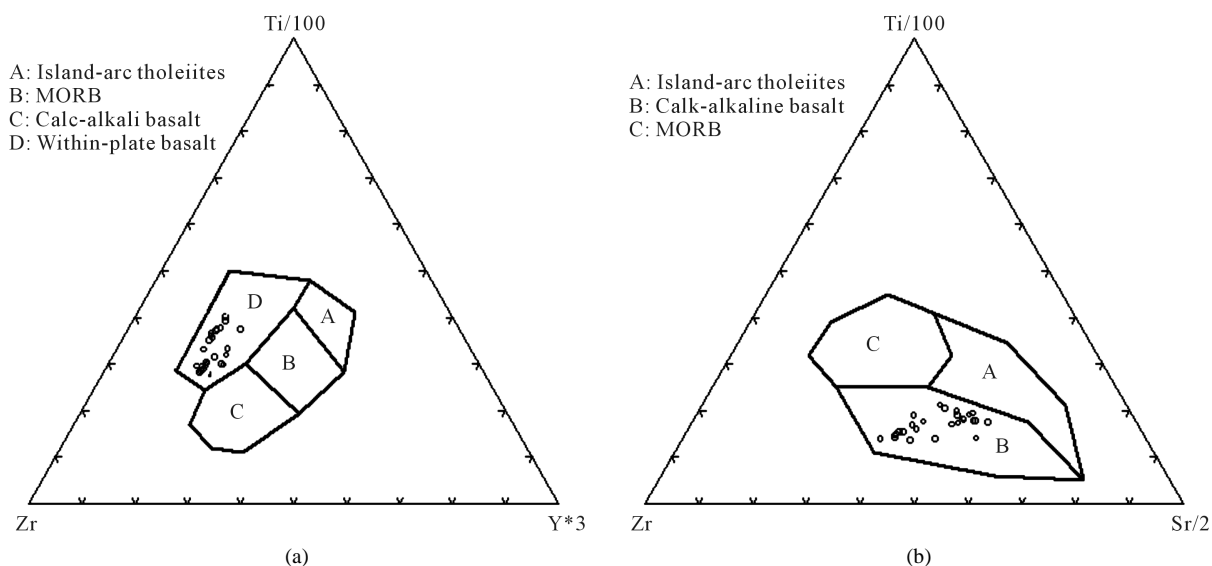
Figure 6. (a) Ti-Zr-Y discrimination diagram for MB [41]; (b) Ti-Zr-Sr discrimination diagram for MB [41].

The geochemical properties of the MB well related, indicating the kind of primitive natural magma that gave rise to the (MB) alkali olivine basalt. The low content of SiO_2 (40.83 - 47.55 ppm) and high content of MgO (6.3 - 11.7 wt%) and total FeO (7.36 - 15.42 wt%) indicated the natural fractionation of the MB. Furthermore, the high concentration of Cr (115 - 324 ppm) is consistent with the earlier findings reported for primary magma (e.g., 257.6 ppm [5], 313.6 ppm [14], 241 ppm [31], and 125.3 ppm [43]). The high Mg≠ (average of 0.52) observed for MB in the present study is similar to that reported earlier for rocks affected by fractionation or accumulation of plagioclase, clinopyroxene, orthopyroxene, and olivine [35]. The Rayleigh fractionation equation is $C_l/C_o = F^{(D-1)}$ [44], where C_l is the concentration of a trace element in the residual melt, C_o is the concentration of a trace element in the original melt, F is the fraction of melt that remains, and D is the bulk partition coefficient. The partition coefficient of Sr and Ba modeled the mineral fractionation vector diagram shown in **Figure 7**, which

indicated that the MB rock samples had fractions of clinopyroxene, orthopyroxene, olivine, and traces of plagioclase.

The degree of partial melting was constant when modeling the concentration of the trace element. The batch melting equation [44] can be given as follows: $C_l/C_o = 1/[D_o + F]^{(1-D_o)}$, where F is the melting degree, C_o and C_l are the concentrations of the elements in the source (original) and liquid, respectively, and D_o is the bulk distribution coefficient of the elements in the initial assemblage and minerals entering into the liquid. By using the distribution coefficient model for Cr and Co [27], the concentration of the large ion lithophile elements (LILE) was found to exhibit primitive composition. The degree of partial melting (F) calculated by using the concentrations of the oceanic crust sources. The studied samples presented an average partial melting degree of around 10%, which is consistent with the previously published results for the Jordanian and Arabian interpolate basalt [5] [12]-[14].

All the above-mentioned geochemical information explain the natural source of major and trace elements patterns in MB, and it is suggested that the mantle source is most likely to be the result of partial melting. This observation is supported by the trace element ratios, such as K/Ba and Zr/Nb ratios [45]. The low content of Y and high TiO_2/Y and Zr/Y ratios indicate that the source is garnet-bearing rocks [34] [46]. The spider diagram for normal mid-ocean ridge basalt (NMORB) for the studied volcanic rocks (**Figure 8(a)**) presented enrichment of the strongly incompatible LILE such as Ba and K, depletion of Nb relatively to K, enrichment of Pb over Ce, and light rare earth elements (LREE) enrichment (La and Ce) over heavy rare earth elements (HREE) and Y, which showed high similarity to MORB. The mafic volcanic MB exhibited negative Nb anomalies and positive Pb anomalies, but presented higher LILE enrichments. The negative anomalies of Ba, Sr, P, and Ti may be attributed to the fractionation of feldspar for Ba and Sr depletion, apatite for P depletion, and (Fe-Ti) oxides for Ti depletion [38]. The primitive mantle value of the rock [47] (**Figure 8(b)**) showed a positive Nb peak, which conforms to the tertiary to recent continental alkali basalt provinces [48] [49] and indicates that the MB is the
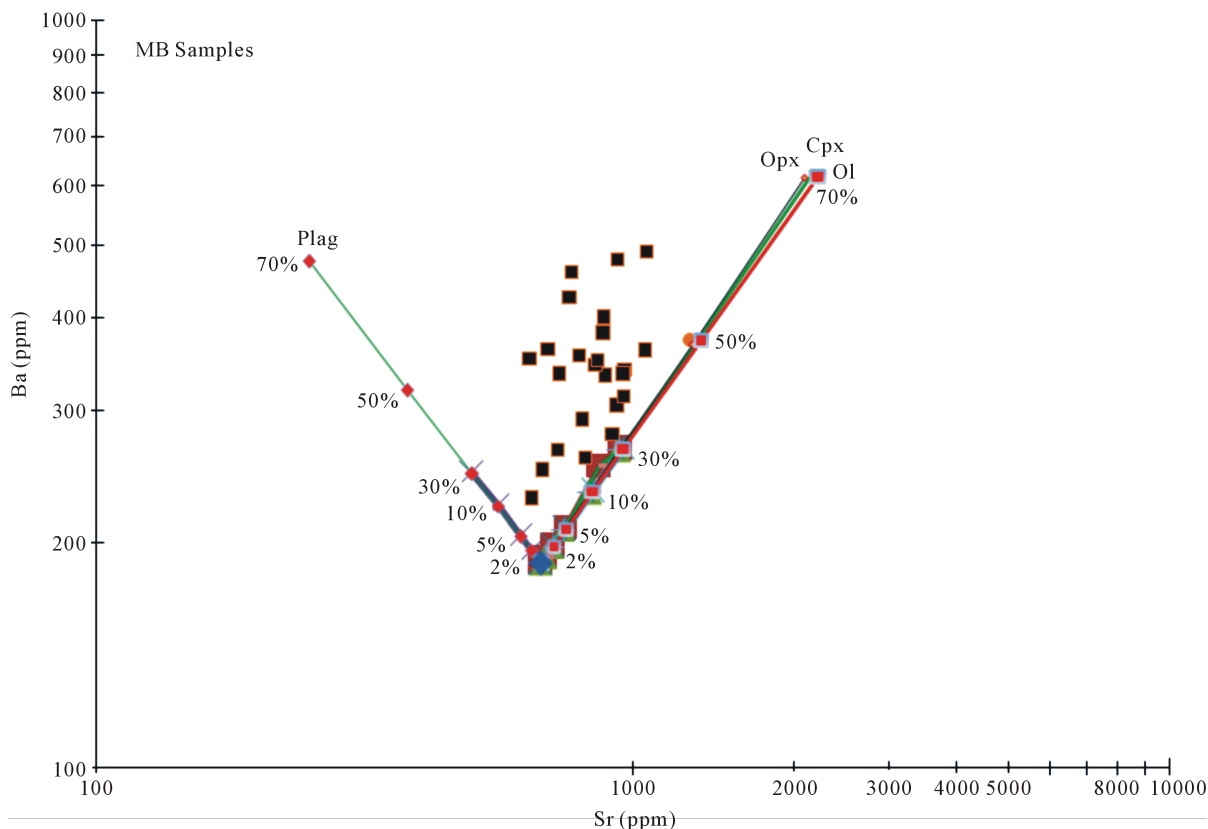

Figure 7. Sr vs. Ba modeled mineral fractionation vector diagram for the MB rock samples studied. Fractionation trends are shown for 2%, 5%, 10%, 30%, 50%, and 70% fractional crystallization of minerals: plagioclase (Plag), clinopyroxene (Cpx), orthopyroxene (Opx), and olivine (Ol).
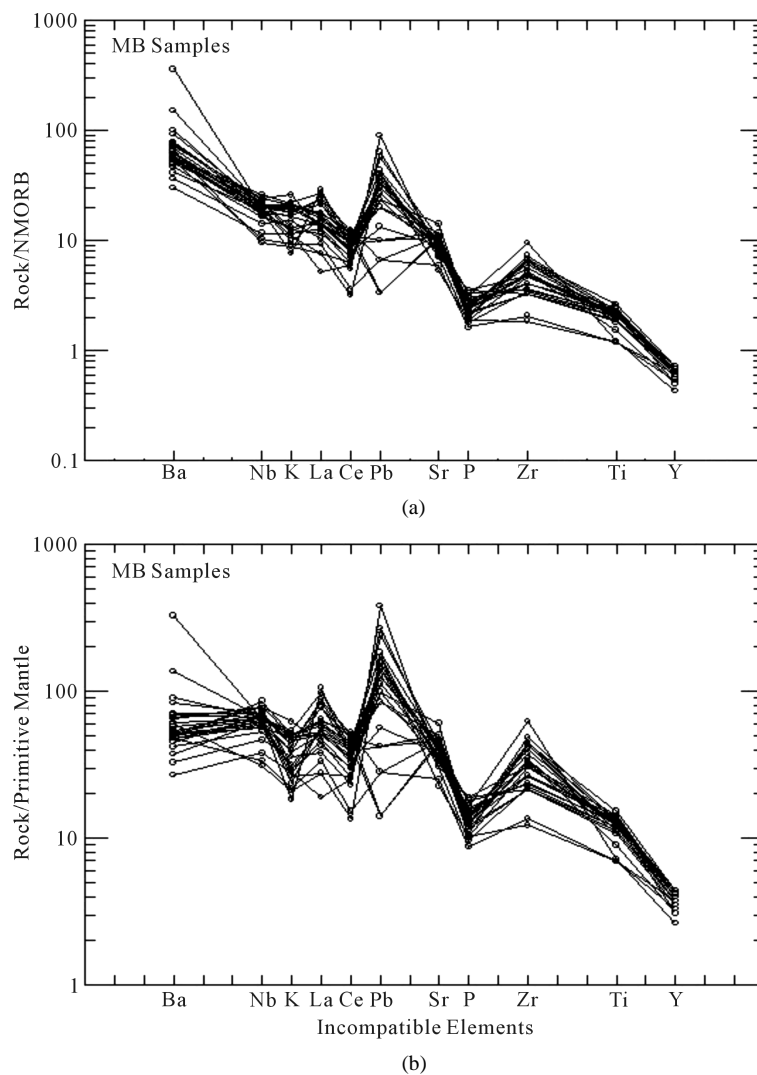
Figure 8. Spider diagram of incompatibility elements from the MB. (a) MORB-normalized trace element plots [51]; (b) Normalized primitive mantle [47]. Trace elements show an increasing trend in the mantle rocks.

product of lithosphere from upwelling asthenospheric mantle [14] [35] [36] [50].

6. Conclusions

The Miocene to Pleistocene (recent) volcanism in central Jordan is produced by intraplate volcanic field. The study area covered Wadi Zaraq-Ma'in along about 15 km east of the Dead Sea. The following conclusions could be drawn from the present study:

1) The mineral composition of MB is as follows: plagioclase, pyroxene, olivine, and opaque minerals (magnetite), with secondary minerals such as calcite, serpentine, and zeolite. The common textures observed were trachytic, glomeroporphyritic, vesicular, and amygdaloidal.

2) The major and trace elements in the MB rock samples were classified based on the basic affinity, intercontinental alkali basalt, and alkaline to calc-alkaline fields.

3) The tectonic setting for the Ti-Zr-Y and Ti-Zr-Sr discrimination diagram showed that the MB samples were within the plate basalt and calc-alkaline basaltic field.

4) The vector diagram for fractional crystallization model for MB showed the presence of clinopyroxene, orthoproxene, olivine, and traces of plagioclase. Furthermore, the distribution coefficient of Cr and Co indicated a

partial batch melting of around 10%.

5) The spider diagram for NMORB and primitive mantle showed enrichment of incompatible LILE such as Ba and K and HREE such as La and Ce, which indicated that MB was a product of lithosphere from upwelling asthenospheric mantle.

Acknowledgements

References

[1] Camp, V. and Roobol, M. (1992) Upwelling Asthenosphere Beneath Western Arabian and Its Regional Implication. *Journal of Geophysical Research*, **97**, 15255-15271. http://dx.doi.org/10.1029/92JB00943

[2] Baker, J., Menzies, M.A., Thirlwall, M.F. and Macpherson, G.G. (1997) Petrogenesis of Quaternary Interpolate Volcanism, Sana'a Yemen: Implication for Plume Lithosphere Interaction and Polybaric Melt Hybridization. *Journal of Petrology*, **38**, 1359-1390. http://dx.doi.org/10.1093/petroj/38.10.1359

[3] White, R. and Mckenzie, D. (1989) Magmatism at Rift Zones the Generations of Volcanic Continental Margins and Flood Basalts. *Journal of Geophysical Research*, **94**, 7685-7729. http://dx.doi.org/10.1029/JB094iB06p07685

[4] Barberi, F., Capaldi, G., Gasperini, P., Marinelli, G., Santacroce, R., Scandone, R., Treuil, M. and Varet, J. (1979) Recent Basaltic Volcanism of Jordan and Its Implications on the Geodynamic Evolution of the Afro-Arabian Rift System. Academia Nazionale Dei Lincei, Att Del Convegni Lincei, Rome, 667-683.

[5] Shaw, J.E., Baker, J.A., Menzies, M.A., Thirlwall, M.F. and Ibrahim, K.M. (2003) Petrogenesis of the Largest Intraplate Volcanic Field on the Arabian Plate (Jordan): A Mixed Lithosphere-Asthenosphere Source Activated by Lithospheric Extension. *Journal of Petrology*, **44**, 1657-1679. http://dx.doi.org/10.1093/petrology/egg052

[6] Ibrahim, K. and Al-Malabeh, A. (2006) Geochemistry and Volcanic Features of Harrat El-Fahda, a Young Volcanic Field in Northwest Arabia, Jordan. *Journal of Asian Sciences*, **127**, 127-154.

[7] Khaled, S. (1996) Ma'in Geological Map, Scale 1:50,000. Natural Resources Authority, Geological Directorate, Amman.

[8] Moffat, D. (1988) A Volcano Tectonic Analysis of the Cenozoic Continental Basalts of Northern Jordan: Implications for Hydrocarbon Prospectively in the Block B Area. Unpublished Report, University College of Swansea, Swansea.

[9] Duffield, W., Mckee, E., El-Salem, F. and Feimeh, M. (1988) K-Ar Ages Chemical Composition and Geothermal Significance of Cenozoic Basalt near the Jordan Rift. *Geothermics*, **17**, 635-644. http://dx.doi.org/10.1016/0375-6505(88)90048-X

[10] Ilani, S., Harlavan, Y., Tarawneh, K., Rabba, I., Weinberger, R., Ibrahim, K., Peltz, S. and Steinitz, G. (2001) New K-Ar Ages of Basalts from the Harrat Asham Volcanic Field in Jordan: Implications for the Span and Duration of Upper Mantle Upwelling Beneath the Western Arabian Plate. *Geology*, **29**, 171-174. http://dx.doi.org/10.1130/0091-7613(2001)029<0171:NKAAOB>2.0.CO;2

[11] Al-Malabeh, A. (1994) Geochemistry of Two Volcanic Cones from the Intercontinental Plateau Basalt of Harrat El-Jaban NE-Jordan. *Geochemistry Journal*, **28**, 517-540. http://dx.doi.org/10.2343/geochemj.28.517

[12] Al-Malabeh, A., El-Hasan, T., Lataifeh, M. and Shea, M. (2002) Geochemical and Mineralogical Related Magnetic Characteristics of the Tertiary-Quaternary (Umm Al-Qutein) Basaltic Flows from the Basaltic Field of Harrat El-Jabban Northeast Jordan. *Physica B*: *Condensed Matter*, **32**, 396-403. http://dx.doi.org/10.1016/S0921-4526(02)01083-9

[13] Shaw, J.E., Baker, J.A., Kent, A.J., Ibrahim, K.M. and Menzies, M.A. (2007) The Geochemistry of the Arabian Lithospheric Mantle—A Source for Intraplate Volcanism. *Journal of Petrology*, **48**, 1495-1512. http://dx.doi.org/10.1093/petrology/egm027

[14] El-Hasan, T. and Al-Malabeh, A. (2008) Geochemistry, Mineralogy and Petrogenesis of El-Lajjoun Pleistocene Alkali Basalt of Central Jordan. *Jordan Journal of Earth and Environmental Sciences*, **1**, 53-62.

[15] Al-Dalou, A. and Ibrahim S. (2001) Regional Geochemical Prospecting for Minerals (Basalt of Ma'in and Er-Rabba Sheet Area). Natural Resources Authority, Amman.

[16] Steinitz, G. and Baratov, Y. (1992) The Miocene-Pleistocene History of the Dead Sea Segment of the Rift in Light or

K-Ar Age of Basalts. *Israel Journal of Earth Sciences*, **40**, 199-208.

[17] Fediuk, F. and Al-Fugha, H. (1999) Dead Sea Region: Fault-Controlled Chemistry of Cenozoic Volcanic Geolines. *Praha*, **9**, 29-34.

[18] Bender, F. (1974) Geology of the Arabian Peninsula, Jordan. *US Geological Survey Professional Paper*, 560-1, 36.

[19] Khaled, S. (1998) The Geology of Ma'in Area Map Sheet No. 3153 III. Natural Resources Authority, Geology Directorate, Geological Mapping Division, Amman, Jordan.

[20] Amer, M.O. (2011) Petrology and Geochemistry of Zarqa-Ma'in Basalts and Their Impact on the Water Chemistry of the Dead Sea. MS Thesis, Yarmouk University, Irbid, 145.

[21] Hatcher, R., Zietz, I., Regan, R. and Abu-Ajammieh, M. (1981) Sinistra Strike-Slip Motion on the Dead Sea Rift: Confirmation from New Magnetic Data. *Geology*, **9**, 458-462.
http://dx.doi.org/10.1130/0091-7613(1981)9<458:SSMOTD>2.0.CO;2

[22] Bentor, Y. (1985) The Crustal Evolution of the Arabo-Nubian Massif with Special Reference to the Sinai Peninsula. *Precambrian Research*, **28**, 1-74. http://dx.doi.org/10.1016/0301-9268(85)90074-9

[23] Stern, R. (1985) The Najed Fault System, Saudi Arabia and Egypt. A Late Precambrian Rift System. *Tectonics*, **4**, 497-511. http://dx.doi.org/10.1029/TC004i005p00497

[24] Bender, F. (1974) Geology of Jordan. Gebrüder Bornträger Verlag, Berlin, 196.

[25] Hollocher, K. (2004) CIPW Norm Calculation Program. Geology Department, Union College.

[26] Kerr, P. (1977) Optical Mineralogy. John Wiley and Sons, New York.

[27] Cox, K., Bell, J. and Pankhurst, R. (1979) The Interpretation of Igneous Rocks. Springer, London.

[28] Le Bas, M.J., Le Maitre, R.W., Steckeisen, A. and Zanettin, B. (1986) A Chemical Classification of Volcanic Rocks Based on the Total Alkali-Silica Diagram. *Journal of Petrology*, **27**, 745-750.
http://dx.doi.org/10.1093/petrology/27.3.745

[29] Thorpe, W. and Graham, P. (1993) A Province Study of Jordanian Basalt Vessels of the Chalcolithic and Early Bronze Age 1 Periods. *Paleorient*, **19**, 51-63. http://dx.doi.org/10.3406/paleo.1993.4596

[30] Cebria, J. and Lopez Ruiz, J. (1995) Alkali Basalt and Levitites in an Extentional Interpolate Setting: The Late Cenozoic Calatrava Volcanic Province (Central Spain). *Lithos*, **35**, 27-46. http://dx.doi.org/10.1016/0024-4937(94)00027-Y

[31] Watts, B.G., Bennett, M.E., Kopp, O.C. and Mattingly, G.L. (2004) Geochemistry and Petrography of Basalt Grindstones from the Karak Plateau, Central Jordan. *Geoarchaeology*: *An International Journal*, **19**, 47-69.

[32] Al-Malabeh, A. (2009) Cryptic Mantle Metasomatism: Evidences from Spinel Lherzolite Xenoliths Al-Harida Volcano in Harrat Al-Shaam, Jordan. *American Journal of Applied Sciences*, **6**, 2085-2092.
http://dx.doi.org/10.3844/ajassp.2009.2085.2092

[33] Jenner, G., Gawood, P., Rautenschlein, M. and White, W. (1987) Composition of Back-Arc Basin Volcanic Valufa Ridge Lau Basin: Evidence for a Slab-Derived Component in Their Mantle Source. *Journal of Volcanology and Geothermal Research*, **32**, 209-222. http://dx.doi.org/10.1016/0377-0273(87)90045-X

[34] Downes, H., Seghed, I., Szakacs, A., Dobasi, G., James, D., Vaselli, O., Rigby, I., Ingram, G., Rex, D. and Peckskay, Z. (1995) Petrology and Geochemistry of Late Tertiary-Quaternary Mafic Alkali Volcanism in Romania. *Lithos*, **35**, 65-81. http://dx.doi.org/10.1016/0024-4937(95)91152-Y

[35] George, S., John, M., Costas, X. and Gavin, H. (2010) Petrogenesis of Latest Miocene-Quaternary Continental Intraplate Volcanism along the Northern Dead Sea Fault System (Al-Ghab-Homs Volcanic Field), Western Syria: Evidence for Lithosphere-Asthenoshere Interaction. *Journal of Petrology*, 1-30.

[36] Wilson, M. (1989) Igneous Petrogenesis. Unwin Hyman Ltd., London, 466.
http://dx.doi.org/10.1007/978-1-4020-6788-4

[37] Clague, D. and Ferry, F. (1982) Petrology and Trace Elements Geochemistry of Honolulu Volcanism: Implication for the Ocean Mantle below Hawaii. *Journal of Petrology*, **23**, 447-504. http://dx.doi.org/10.1093/petrology/23.3.447

[38] Moghazi, A.M. (2003) Geochemistry and Petrogenesis of a High-K Calc-Alkaline Dokhan Volcanic Suite, South Safaga Area, Egypt: The Role of Late Neoproterozoic Crustal Extension. *Precambrian Research*, **125**, 161-178.
http://dx.doi.org/10.1016/S0301-9268(03)00110-4

[39] Middelmost, E. (1975) The Basalt Clan. *Earth-Science Reviews*, **11**, 337-564.
http://dx.doi.org/10.1016/0012-8252(75)90039-2

[40] Winter, J.D. (2001) An Introduction to Igneous and Metamorphic Petrology. Prentice Hall Inc., Upper Saddle River, 697.

[41] Pearce, J.A. and Cann, J.R. (1973) Tectonic Setting of Basic Volcanic Rocks Determined Using Trace Element Analyses. *Earth and Planetary Science Letters*, **19**, 290-300. http://dx.doi.org/10.1016/0012-821X(73)90129-5

[42] Le Maitre, R.W., Bateman, P., Dudek, A., Keller, J., Lameyre Le Bas, M.J., Sabine, P.A., Schmid, R., Sorensen, H., Streckeisen, A., Woolley, A.R. and Zanettin, B. (1989) A Classification of Igneous Rocks and Glossary of Terms. Blackwell, Oxford.

[43] Al-Fugha, H. and Al-Amaireh, M. (2007) Petrology and Origin of Ultramafic Xenoliths from Northeastern Jordan Volcanoes. *American Journal of Applied Sciences*, **4**, 491-495. http://dx.doi.org/10.3844/ajassp.2007.491.495

[44] Rollinson, H.R. (1993) Using Geochemical Data: Evaluation, Presentation, Interpretation. Longman Scientific and Technical, England.

[45] Peltz, S. and Bratosia W. (1986) New Data on the Geochemistry of the Quaternary Basalts in Pensani Mountains. *D. S. Inst. Geophics.*, **71**, 389-403.

[46] Frey, F.A., Green, D.H. and Roy, S.D. (1978) Integrated Models of Basalt Petrogenesis: A Study of Quartz Theoliites to Olivine Melilites from South Eastern Australia Utilizing Geochemical and Experimental Petrological Data. *Journal of Petrology*, **19**, 463-513. http://dx.doi.org/10.1093/petrology/19.3.463

[47] Sun, S.S. and MacDonough, W.F. (1989) Chemical and Isotopic Systematic of Oceanic Basalts Implications for Mantle Composition and Processes in Magmatism in the Ocean Basins. *Geological Society*, *Special Publication*, **42**, 313-345.

[48] Norry, M.J. and Fitton, J.G. (1993) Compositional Differences between Oceanic and Continental Basic Lavas and Their Significance. In: Hawkesworth, C.J. and Norry, M.J., Eds., *Continental Basalts and Mantle Xenoliths*, Shiva Publishing Ltd., Cheshire, England, 5-19.

[49] El-Akhal, H. (2004) Contribution to the Petrography, Geochemistry and Tectonic Setting of the Basalt Flows of the Umm-Qais Plateau, North Jordan. *Geological Bulletin of Turkey*, **47**, 1-10

[50] Thompson, R.N. (1987) Phase Equilibria Constraints on the Genesis and Magmatic Evolution of Oceanic Basalts. *Earth Science Reviews*, **24**, 161-210. http://dx.doi.org/10.1016/0012-8252(87)90023-7

[51] Pearce, J., Harris, N. and Tindle, A. (1984) Trace Element Discrimination Diagram for the Tectonic Interpretation of Granitic Rocks. *Journal of Petrology*, **25**, 956-983. http://dx.doi.org/10.1093/petrology/25.4.956